Numerical Evaluation and Improvement Efficiency of Radial Flow Moving-Bed Reactors for Catalytic Pyrolysis of Light Hydrocarbons to Low Carbon Olefins

Fang-Zhi Xiao,[1] Houyang Chen[2] and Zheng-Hong Luo[2,3]*

1. *Department of Chemical and Biochemical Engineering, College of Chemistry and Chemical Engineering, Xiamen University, Xiamen 361005, P. R. China*
2. *Department of Chemical Engineering, Shanghai Jiao Tong University, Shanghai 200240, P. R. China*
3. *State Key Laboratory of Coal Conversion, Institute of Coal Chemistry, Chinese Academy of Sciences, Taiyuan 030000, P. R. China*

A three-dimensional (3D) reactor model based on the Eulerian-Eulerian approach was applied to describe the gas-solid flow and heat transfer performance in a radial flow moving bed reactor (RFMBR). A six-lumped kinetic model for the catalytic pyrolysis of C_4 hydrocarbon was employed. The heat transfer characteristics and species concentration profiles were investigated in the reactor under various reaction conditions. Effects of operation parameters and reactor structures on the reactor performance were also evaluated and optimized numerically. Simulation results show that there exists a good heat transfer performance between gas and solid phases in the catalyst bed. The temperature profiles and the species yield distributions are different with respect to bed height positions. Moreover, the results indicate that product yield is more sensitive to the reaction temperature than to the dilution rate and the reaction residence time. For the Z-type centripetal flow RFMBR, an annular tube with an inverted cone structure is helpful to improve the uniformity of flow distribution and increase low-carbon olefins yields.

Keywords: RFMBR, catalytic pyrolysis of light hydrocarbon, CFD modelling, optimization

INTRODUCTION

Light olefins (such as propylene and ethylene) as petrochemical basic organic materials are always used to produce polyolefin. With the rapid development of the petrochemical industry, the demand for light olefins has been growing dramatically in China.[1–4] In general, two common processes for producing light olefins are steam pyrolysis of naphtha, and catalytic cracking of heavy oil.[5–11] However, steam pyrolysis and catalytic cracking suffer from high energy consumption and low yield of light olefins, respectively.

In order to improve the yield of light olefins and reduce energy consumption, researchers have extended the sources of raw materials and developed a process of catalytic pyrolysis of light hydrocarbons to low-carbon olefins,[6] where highly active and selective catalysts are used to improve propylene and ethylene yields, and to reduce the yields of low value-added by-products such as methane. Compared with the steam pyrolysis process, the reaction temperature is lower, resulting in lower energy consumption. In addition, for the catalytic pyrolysis process, the distribution of the products can be adjusted flexibly by controlling the operating conditions.

Until now, some investigations of the catalytic pyrolysis of light hydrocarbons to low carbon olefins were reported. However, most of them focused on fixed bed reactor or fluidized bed reactor (FBR) experiments.[5–11] Basu and Kunzru[7] investigated thermal pyrolysis and catalytic pyrolysis of naphtha in a fixed bed reactor. Sang et al.[12,13] studied the catalytic pyrolysis of naphtha over a KVO_3/α-Al_2O_3 catalyst in a vacant tube reactor. Zhang et al.[14] studied the reaction behaviour of FCC gasoline catalytic pyrolysis to light olefins in a FBR, and investigated the effects of operation conditions such as reaction temperature and residence time on reaction behaviour. Li et al.[15] investigated the reaction behaviour of catalytic pyrolysis of C_4 hydrocarbons experimentally. Additionally, some kinetic research concerning the catalytic pyrolysis of light hydrocarbons was also conducted. Chen et al.[16] performed a series of experiments in a riser reactor to study the secondary reaction process of FCC gasoline with different operation conditions. An eight-lump kinetic model was proposed to describe this reaction process, and the calculated results agree well with the experimental results. Meng et al.[17] established a six-lump kinetic model to describe the reactions with appropriate assumptions.

Based on the discussions above, catalytic pyrolysis of light hydrocarbons is an effective method to produce low-carbon olefins. For the reaction of catalytic pyrolysis of light hydrocarbons, the deactivation of the catalyst is slow due to low carbon content of feedstock. A reactor with the characteristics of continuous regeneration and a long cycle of catalyst particles may be suitable for the reaction of catalytic pyrolysis light hydrocarbons. However, for the reactors used in former studies, the fixed bed reactor contains poor production continuity, while the FBR is suitable for fluidization technology since it is characteristic in frequent regeneration of catalyst particles. Consequently, both the fixed bed reactor and the FBR are not suitable for catalytic pyrolysis of light hydrocarbons.[18,19] The radial flow moving bed reactor (RFMBR), with the advantages of "high flow capacity, low pressure drop, permitted use of

* *Author to whom correspondence may be addressed.*
E-mail address: luozh@sjtu.edu.cnluozh@sjtu.edu.cn
Can. J. Chem. Eng. 93:1033–1043, 2015

DOI 10.1002/cjce.22187
Published online 24 April 2015 in Wiley Online Library (wileyonlinelibrary.com).

small-particle catalysts, low particle attrition rate, uniform contact between fluid and solids, continuous regeneration of catalyst particles, and wide variation in solids residence time,"[20] is demonstrated to match the characteristics of catalytic pyrolysis of light hydrocarbons and may be used with the catalyst effectively. Therefore, RFMBRs are more suitable for the reaction of catalytic pyrolysis of light hydrocarbons to low-carbon olefins.

In this work, a 3D two-phase flow-reaction model containing the Eulerian-Eulerian approach and the kinetic theory of granular flow as well as a six-lump reaction kinetic equation is applied to describe the reaction of catalytic pyrolysis of light hydrocarbons in a CP-Z flow radial moving bed reactor. The reactor behaviours such as the distribution of temperature and species concentration are predicted. In order to provide necessary information for the optimal design and operation of the catalytic pyrolysis process of light hydrocarbons, the effects of the reactor structures and operation conditions on the reactor performance are thoroughly investigated.

SIMULATION OF THE CP-Z RFMBR

In this simulation, the selected CP-Z RFMBR is the same as that reported in the work of Song et al.[20] According to Song et al., a complete 3D physical model was established. The selected reactor has a length of 2 m, and consists of two perforated cylinders and a reactor wall. The perforated cylinders are replaced by a thin packed bed. The reactor can be divided into three sections: the centre channel, the annular channel, and the catalyst bed channel between two coaxial cylinders. Then, structured quadrilateral and hexahedral grids were applied to the radial and axial directions of the annular channel and the catalyst bed channel, respectively. The radial direction of the centre channel was meshed with the triangular grid and the axial direction of the centre channel was meshed with the pentahedral grid. More detailed information regarding the reactor configuration and dimensions is provided in Figure 1 and Table S1.

The gaseous reactants are continuously fed into the reactor from the annular channel inlet, then flow radially across the catalyst bed centripetally, and finally flow out of the centre channel.

MATHEMATICAL MODEL AND SIMULATION METHOD

Mathematical Model

A model consisting of a complete 3D CFD Eulerian-Eulerian two-fluid model and the Ergun resistance equation is developed to describe the flow behaviour in CP-Z flow radial moving bed reactor. Herein, both phases are considered to be continuous and fully interpenetrating. The two-fluid model is closed using the kinetic theory of granular flow, and the resistance offered by the porous walls of the centre and annular pipes are described by Ergun resistance equation. The main governing equations are summarized in Table S2.[21–24] On the other hand, the six-lump reaction kinetic model suggested by Meng et al.[17] was used to describe the complex catalytic pyrolysis reaction of C_4 hydrocarbon. "The C_4 hydrocarbons were divided into two lump species, butene and butane, because the cracking performance of butene differs from that of butane."[17] The targeted products, ethene and propene, were considered as two lumps. For the by-products hydrogen and light alkanes, because of their low yields and similar formation mechanisms, they are considered as one lump. Coke and liquid components were categorized as one lump due to both coke and liquid being the products of polymerization, aromatization, and condensation. More information regarding reaction networks, the properties of feedstock and their kinetic parameters are shown in Figure 2 and Tables S3–S4, respectively. The reaction rate R_i of a gaseous i is defined as

$$R_i = k_i(\rho_g C_i)\frac{\rho_s}{\varepsilon}, \tag{1}$$

$$\text{where} \quad k_i = k_{0i}\exp(-\frac{E_i}{RT}). \tag{2}$$

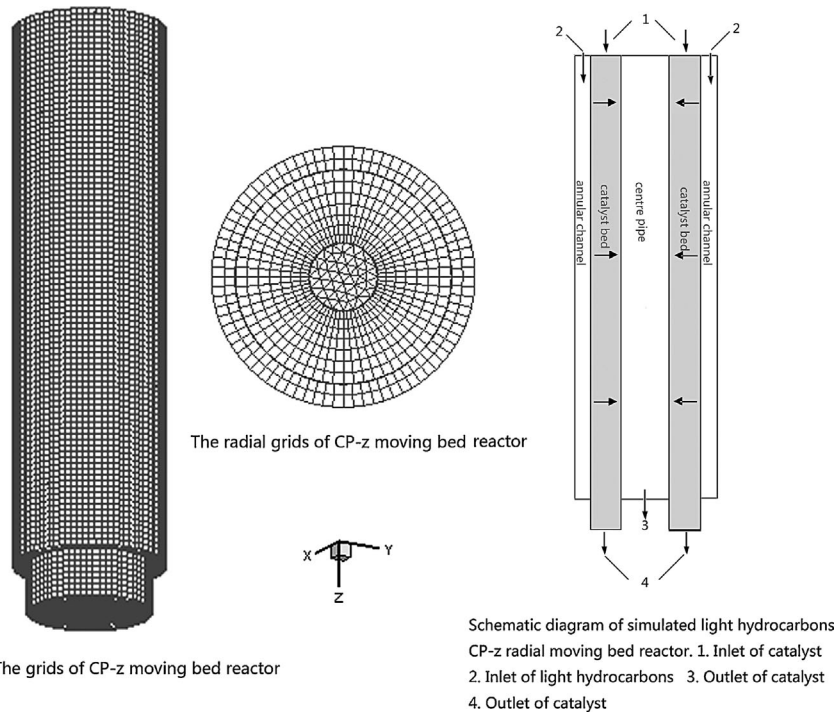

Figure 1. Physical model and grids of 3D CP-Z radial flow moving bed reactor.

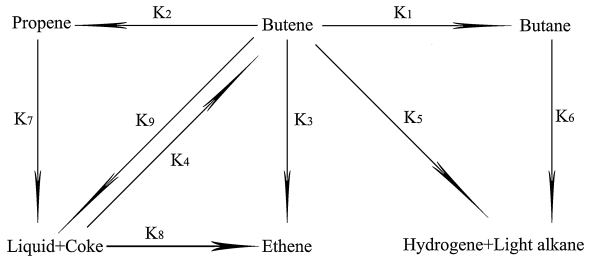

Figure 2. Reaction network of the 6-lump kinetic model.

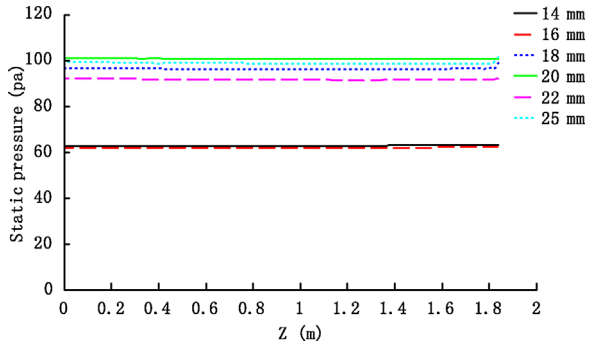

Figure 3. Static pressure distribution in the annular channel of CP-z radial flow moving bed reactor at different mesh size resolutions (simulation conditions: $v_{g,inlet} = 0.86$ m/s, $v_{s,inlet} = 0.001$ m/s, $\varepsilon = 0.37$, $P = 1.01 \times 10^5$ Pa).

In addition, the auxiliary formula of the gas mixture, standard molar enthalpy of formation, and molar heat capacity of lumps are listed in Tables S5–S7.[25–28]

Simulation Method

The model is used to simulate the complex two-phase flow and the catalytic pyrolysis reaction of light hydrocarbons to low carbon olefins. In this work, the 3D simulations of the above model were performed with the commercial CFD software FLUENT 6.3.26 (Ansys Inc., USA) in double precision mode. A commercial grid-generation tool, GAMBIT 2.3.16 (Ansys Inc., USA) was used to generate the 3D models of the reactor and the computational grids, as shown in Figure 1. Source terms in different governing equations were specified by User-Defined Functions using C programming language, then were coupled and hooked into the FLUENT solver.

The inlet velocity was set for both the gas phase and the solid phase. "Pressure outlet" boundary was used at the outlet, and exit pressure was specified. At the wall, no-slip boundary conditions were set. More detailed information regarding the model parameters and boundary conditions is provided in Tables S8–S9.[22,23,29]

RESULTS AND DISCUSSION

Grid Independency and Model Verification

To confirm that the CFD results are independent of the grid size, simulations of the CP-Z flow configuration with mesh sizes of 25, 22, 20, 18, 16, and 14 mm are performed at the cold model conditions (see Table S10). Since static pressure is an important parameter in a reactor, its distributions along the annular channel are used to monitor numerical errors, as shown in Figure 3. From Figure 3 there is no obvious difference between the cases using the grid sizes of 16 mm and 14 mm. In addition, the fine mesh (16 mm and 14 mm) cases capture more real static pressure in this reactor than the coarse mesh (18, 20, 22, and 25 mm) cases. Moreover, cases using the grid sizes of 16 mm and 14 mm obtain similar static pressure in the annular channel. Therefore, the grid size of 16 mm is sufficiently fine for providing reasonably mesh-independent results, and is selected as a base case and applied in the rest of the article.

Although the reaction kinetic model adopted in this work is deduced at a lab scale, it also can be used in our reactor due to few influences of reactor type on the bulk reaction kinetic mechanism. Moreover, it has been certified that the selectivity of ethylene and propylene as well as light hydrocarbons conversion are similar during the cracking process in both moving bed reactors and fixed bed reactors, which indicates that the kinetic character in the fixed bed is similar to the moving bed reactor at the same reaction cases.[30] Herein, the experiment data from the work of Meng et al.[17] are used to validate the simulation data (Table S11), which demonstrate that there is good agreement between the simulation and experiment data.

Heat Transfer Characteristics and Species Concentration Profiles

Temperature profile in the reactor

Figure 4 shows the temperature profiles of gas and solid phases in the reactor. From Figure 4, the reactant temperatures in the annular channel and the centre channel remain almost constant, while they increase gradually along the flow direction in the catalyst bed, and reach about 770 K. The temperature gradient decreases continually along the direction of the catalyst bed. In addition, as the reactants from the annular channel flow into the catalyst bed, the total mass flow increases along the catalyst bed. This leads to contact between reactants with low temperature

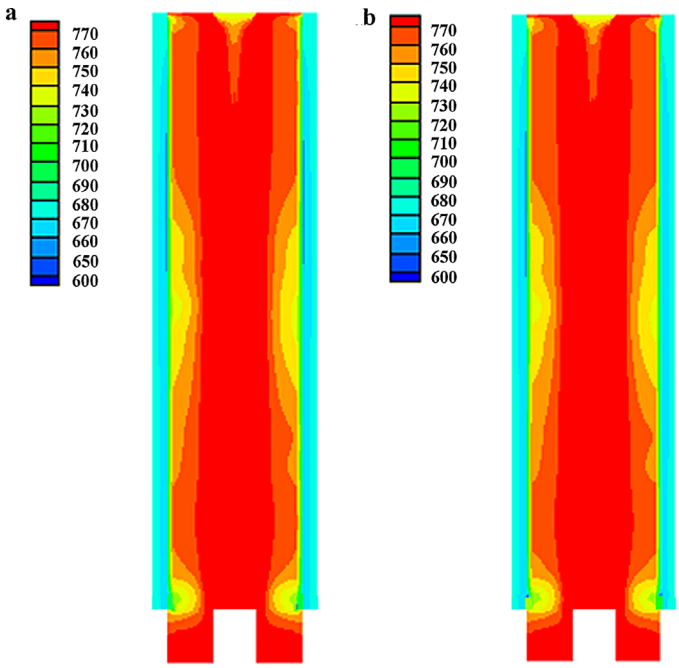

Figure 4. Temperature profiles of gas phase and solid phase in the reactor (simulation conditions: $T_{gas\_inlet} = 673.15$ K, $T_{cat\_initial} = 773.15$ K).

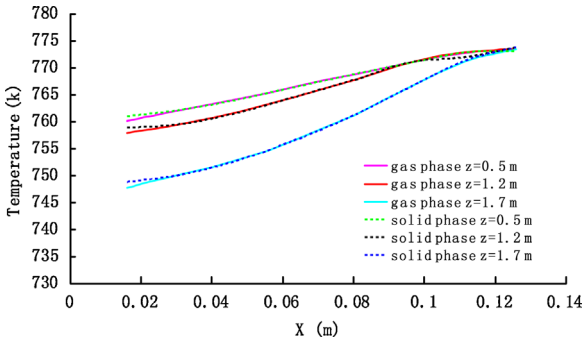

Figure 5. Temperature profiles of gas phase and solid phase in catalyst bed at different heights of reactors (simulation conditions: $T_{gas\_inlet} = 673.15$ K, $T_{cat\_initial} = 773.15$ K).

and those catalysts loaded in the bed with high temperature. Since there is a large temperature difference between the reactant gas and catalyst particles, a strong heat transfer between them will be produced. Meanwhile, an endothermic cracking reaction occurs at these catalyst surfaces. As a result, the above coupling effects lead to complex temperature profiles in the middle and at the bottom of the catalyst bed.

Figure 5 shows the temperature profiles of gas and solid phases in the catalyst bed at different reactor heights. Herein, the upper surface of the catalyst bed serves as a reference plane: the position in the catalyst bed is represented by the distance away from the reference plane (similarly hereafter). As described in Figure 5, only a slight temperature difference (less than 1.5 K) exists between the gas and solid phases in the catalyst bed at the same reactor height. This is attributed to the high heat transfer rate between the two phases. Since the temperature difference is slight between the two phases, a macroscopic heat transfer equilibrium state is established. In addition, the temperature profiles of gas and solid phases in the catalyst bed at different reactor heights show great difference.

Species concentration profiles

Figures 6–7 show the concentration profiles of products and of reactants along the reactor, respectively. From Figure 6, the mass fractions of light alkane + H_2, liquid + coke, ethylene, and propylene increase along the flow direction in the catalyst bed. As shown in Figure 7, the mass fraction of butene decreases along the flow direction in the catalyst bed, while the mass fraction of butane shows the opposite trend. Herein, a low temperature operating condition is employed in this case, and the generation rate of butane is larger than its consumption rate, which results in the above distribution. In order to study the distribution of species concentration at different heights of the reactor, the positions of z=0.5 m, z=1.2 m, and z=1.7 m are selected to investigate the distribution of species concentration.

Figures 8–9 plot the concentration distribution of products and reactants conversion along the flow direction of the catalyst bed at different reactor heights, respectively. It can be observed from Figures 8–9 that there also exists some difference of species conversion/yield distributions at different reactor heights, especially at the lower half of the reactor. The degree of catalytic pyrolysis decreases along the reactor due to a higher radial velocity and a shorter residence time of gas phase, which leads to the decrease of species conversion/yield along the reactor. From Figure 8c, ethylene yield increases along the flow direction of the catalyst bed, while the growth rate decreases gradually. Propylene yield increases significantly in the first half of the catalyst bed, and then increases slightly. In the last one-third of the bed, propylene yield almost keeps stable (see Figure 8d). As final products, the total yield of light alkane + H_2 increases progressively (see Figure 8a). Moreover, as shown in Figure 9b, butene (as the primary feedstock) cracks rapidly in the first one-third of the catalyst bed due to a higher reactant concentration.

Optimization of Operating Conditions

Reaction temperature

The concentration distributions of products along the flow direction of the catalyst bed with different reaction temperatures

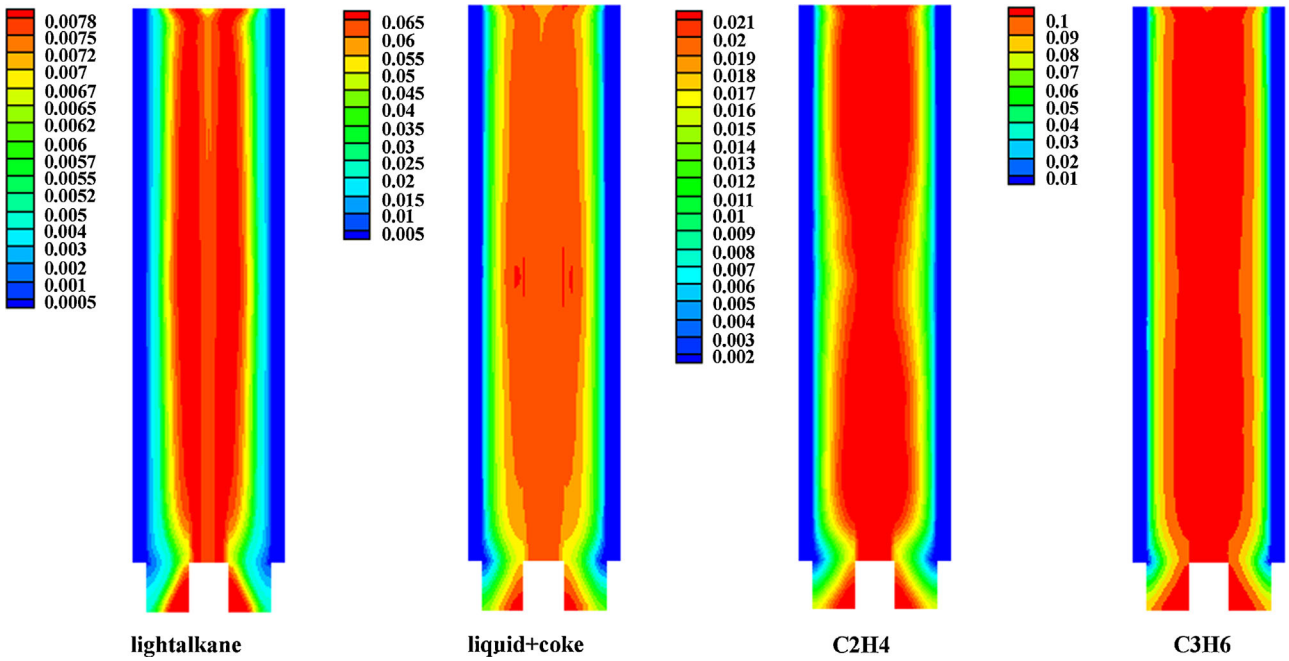

Figure 6. Concentration profiles of products along the reactor (simulation conditions: $T_{gas\_inlet} = 673.15$ K, $T_{cat\_initial} = 773.15$ K).

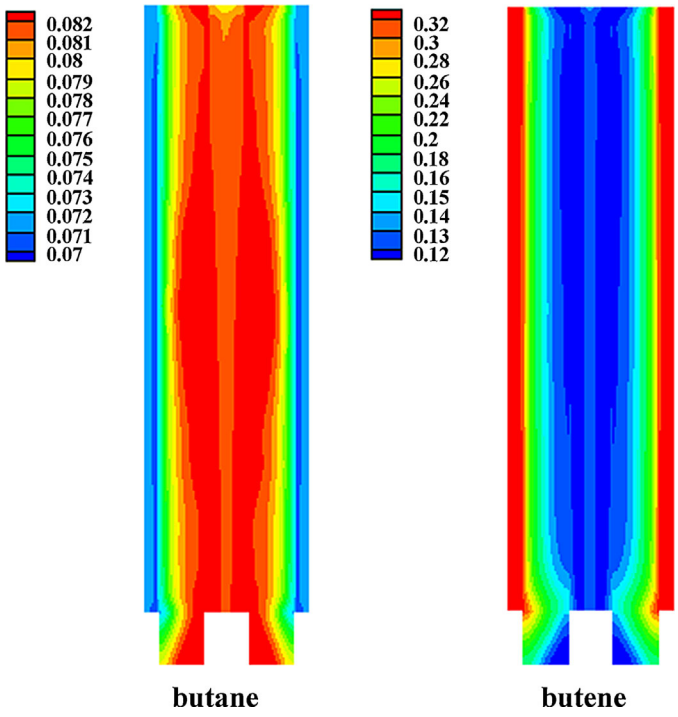

Figure 7. Concentration profiles of reactants along the reactor (simulation conditions: $T_{gas\_inlet} = 673.15$ K, $T_{cat\_initial} = 773.15$ K).

are shown in Figure 10. The reaction temperature is adjusted by varying initial catalyst temperature. The position z = 1.2 m is selected to investigate the products yield and the reactants conversion (similarly hereinafter). Figure 10a illustrates that the yield of light alkane + H_2 increases with increasing the initial catalyst temperature. Increasing initial catalyst temperature introduces more heat into the reactor which leads to a higher reaction temperature. In addition, the reaction of catalytic pyrolysis of C_4 hydrocarbon to light alkane + H_2 is an endothermic process, so as a result, light alkane + H_2 yield increases with increasing the reaction temperature. Figures 10c–d indicate that when increasing the initial catalyst temperature from 773.15 K to 923.15 K, the yields of ethylene and propylene increase, whereas the yields of ethylene and propylene decrease as the initial catalyst temperature increases from 923.15 K to 973.15 K. Compared with the yield of propylene, the yield of ethylene increases quickly. In catalytic pyrolysis of C_4 hydrocarbon, ethylene and propylene are intermediate products. With the increasing of the initial catalyst temperature, the reaction temperature increases, and higher reaction temperature leads to a higher production rate of ethylene and propylene, which lead to higher concentrations of ethylene and propylene. When the concentrations of ethylene and propylene reach a sufficiently large value, the consumption rates of ethylene and propylene are larger than their production rates. Therefore, the yields of ethylene and propylene decrease when the reaction temperature is over a critical value. The liquid + coke yield generally decreases with increasing the initial catalyst temperature (see Figure 10b). Dimerization of butene is an exothermic process, while cracking of liquid products is an endothermic process. By increasing the reaction temperature, the production rate of liquid + coke decreases while the consumption

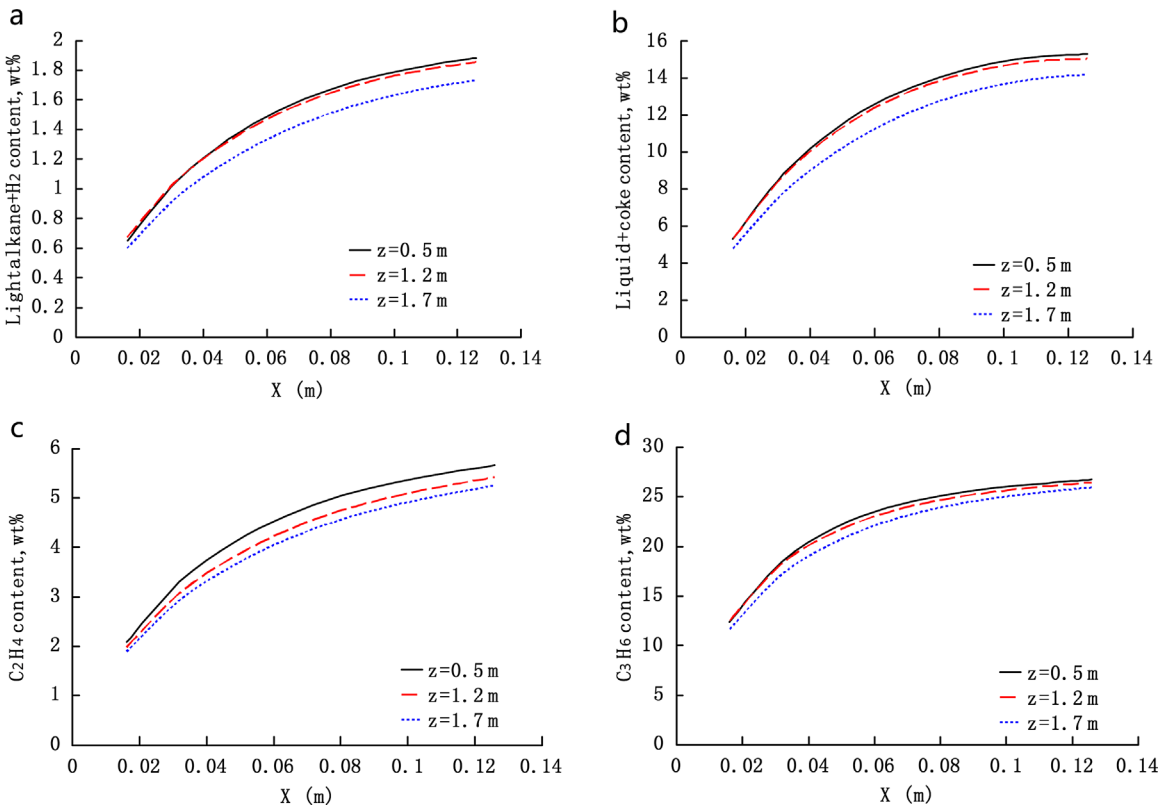

Figure 8. Concentration distribution of products along the flow direction in catalyst bed at different heights of reactor: (a) light alkane + H_2, (b) liquid + coke content, (c) ethylene, (d) propylene (simulation conditions: $T_{gas\_inlet} = 673.15$ K, $T_{cat\_initial} = 773.15$ K).

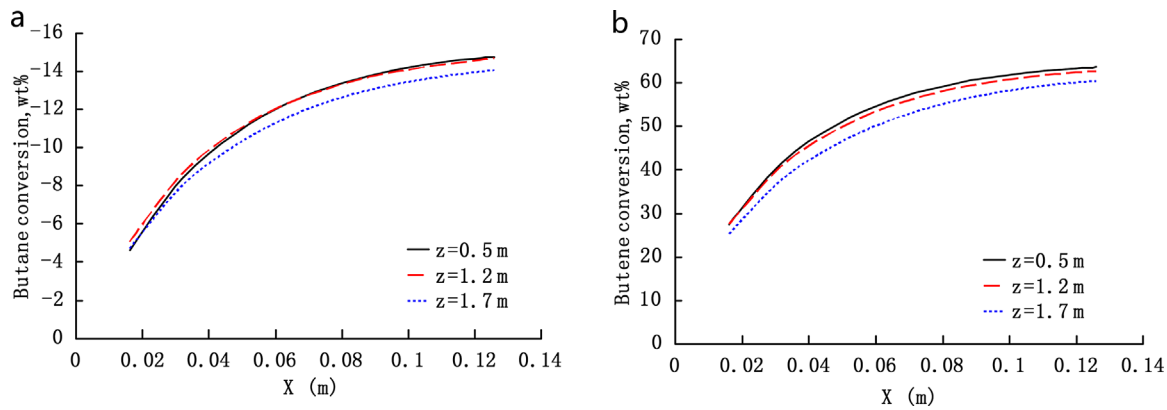

Figure 9. Reactant conversion along the flow direction in catalyst bed at different heights of reactor (simulation conditions: $T_{gas\_inlet} = 673.15$ K, $T_{cat\_initial} = 773.15$ K).

rate of liquid + coke increases. Therefore, the yield of liquid + coke decreases.

Residence time

Figures 11–12 show the concentration distribution of products and reactants conversion along the flow direction of the catalyst bed with different residence time. Residence time is adjusted by varying the width of the catalyst bed, and widths of 0.119, 0.139 and 0.159 m are used. One can observe from Figure 11 that the yields of these products increase with catalyst bed width increases. Compared with ethylene and propylene, the yields of liquid + coke and light alkane + H_2 increase more quickly. In addition, the yields of ethylene and propylene increase slowly when increasing the width of catalyst bed. In catalytic cracking of C4 hydrocarbon, ethylene and propylene are intermediate products. Long residence time of reactants leads to high concentrations of ethylene and propylene, which restrain their generation and accelerate consumption. For the reactor in this study, the concentrations of ethylene and propylene can reach a large value when the width of catalyst bed is 0.119–0.139 m. Therefore, it is useless for enhancing ethylene and propylene yields when continuing to increase the width of catalyst bed. The influence of residence time on reactant conversion is shown in Figure 12. As the residence time increases, both the conversion rates of butene and butane increase. However, the increasing conversion of reactants mainly converts to the by-products. Accordingly, the residence time plays

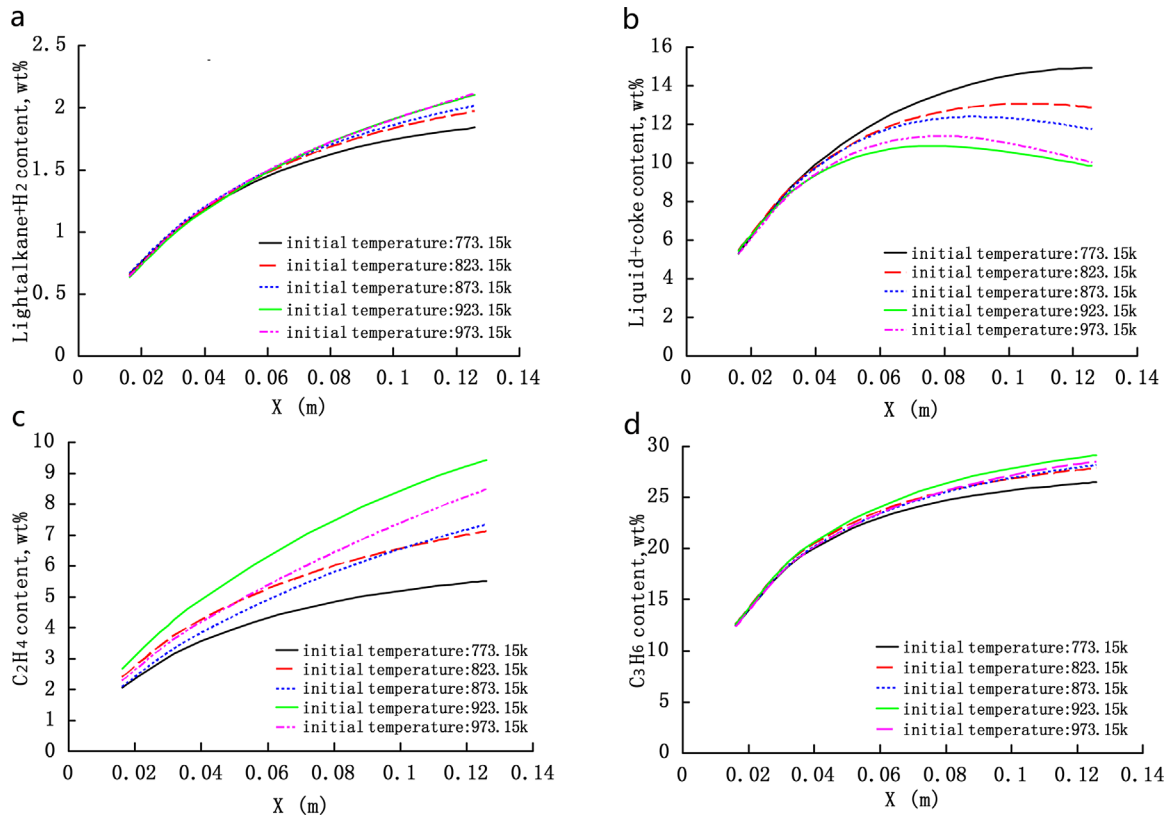

Figure 10. Concentration profiles of product distribution along the flow direction in catalyst bed with different reaction temperatures.

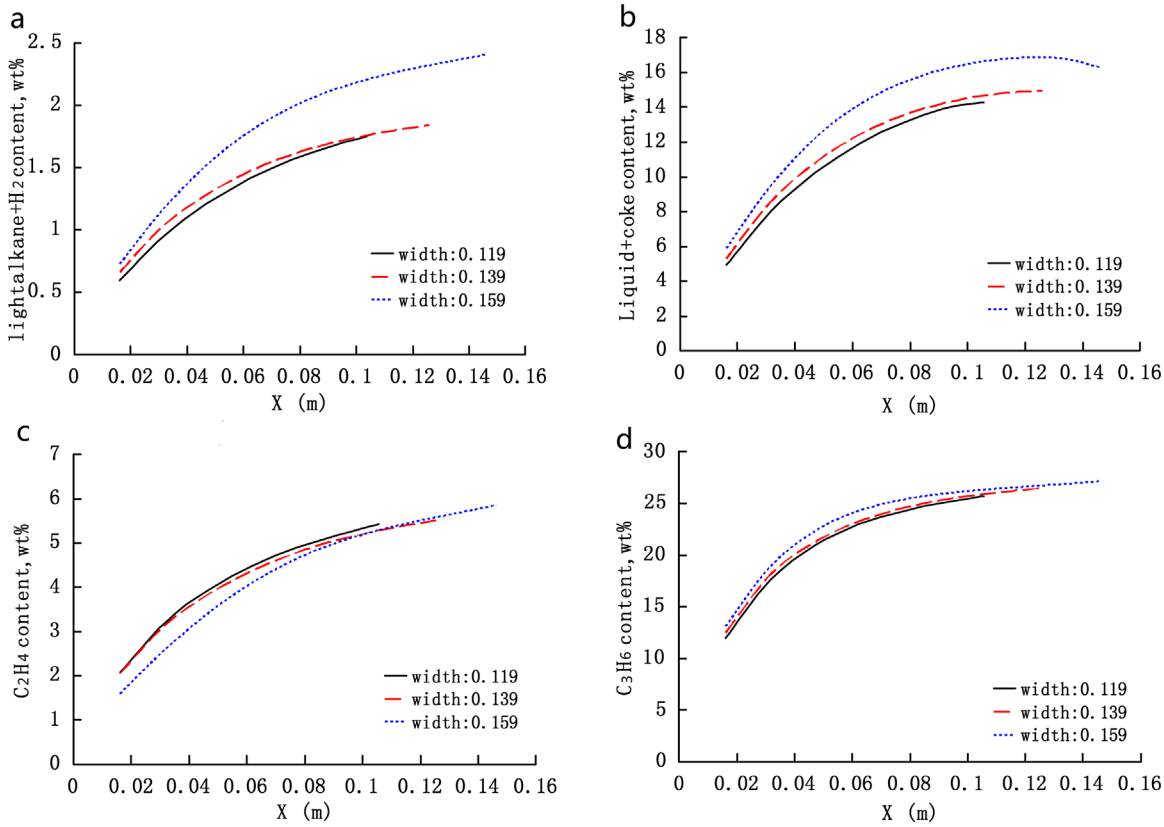

Figure 11. Concentration distribution of products along the flow direction in catalyst bed with different residence times.

an important role in the catalytic cracking reaction. In addition, when the width of catalyst bed is larger than 0.139 m, the yields of by-products increase more quickly than the objective products. Therefore, with the consideration of the conversion rate and the objective products, the most appropriate width of catalyst bed used in this study is between 0.119 m and 0.139 m.

Optimization of Reactor Structure

From the above sections, there always exists some difference of the flow field distribution at different reactor heights. Generally, the improvement method is to enhance the absolute value of the pressure drop between the annular and centre channel, but this will consume more energy. Huang et al.[31] used a choke device to improve the flow uniformity by changing the cross-sectional area of the discharge channel. According to the theory above, in this work, the annular tube using an inverted cone structure and the 2 ° dip angle as well as the optimum operating conditions are used to investigate the flow uniformity in this reactor.

Figure 13 shows that the normalized pressure drops along the reactor with normal and inverted cone structures. We can observe that the normalized pressure drop along the reactor is always 1 for the uniform flow. Moreover, the reactor with inverted cone structure can achieve more uniform flow than the reactor with normal structure. For the inverted cone structure, the flow cross-sectional area of the annular channel and mass loss decrease along the reactor, which leads to a large pressure drop in the annular

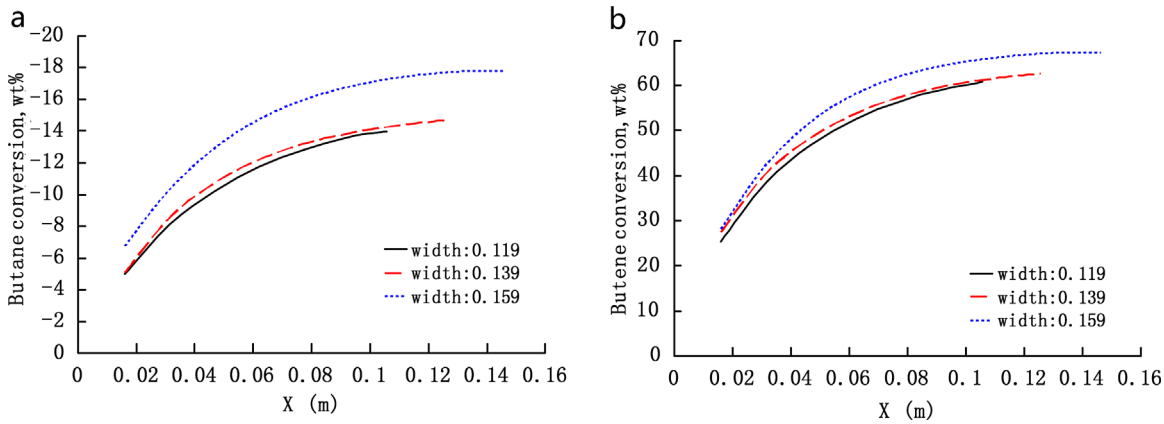

Figure 12. Reactant conversion along the flow direction in catalyst bed with different residence times.

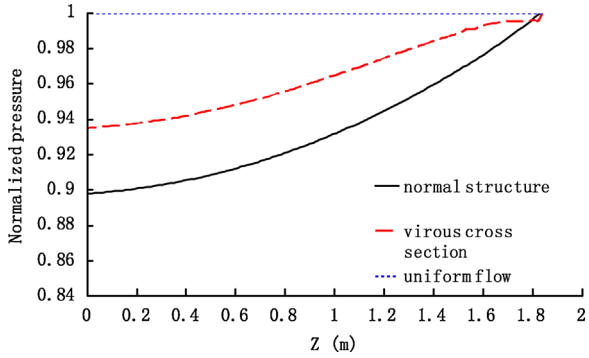

Figure 13. Normalized pressure drop along the reactor with normal and inverted cone structures.

channel and a closer pressure distribution between the annular and centre channels. The distribution of gas temperature along the flow direction of the catalyst bed at different heights of reactor with normal and inverted cone structures is shown in Figure 14. From Figure 14, the gas temperature profiles at different heights of the reactor with inverted cone structure are closer than those with normal structure. In practice, the residence time increases with the decreasing of the radial pressure drop, which leads to a large increase of gas temperature in the first half of the catalyst bed.

Figures 15–18 show the distribution of species conversion/yield along the flow direction of the catalyst bed at different heights of reactor with normal and inverted cone structures. Comparing Figures 15 and 16 to Figures 17 and 18, the distributions of species conversion/yield along the flow direction of the catalyst bed at different reactor heights with inverted cone structure are more

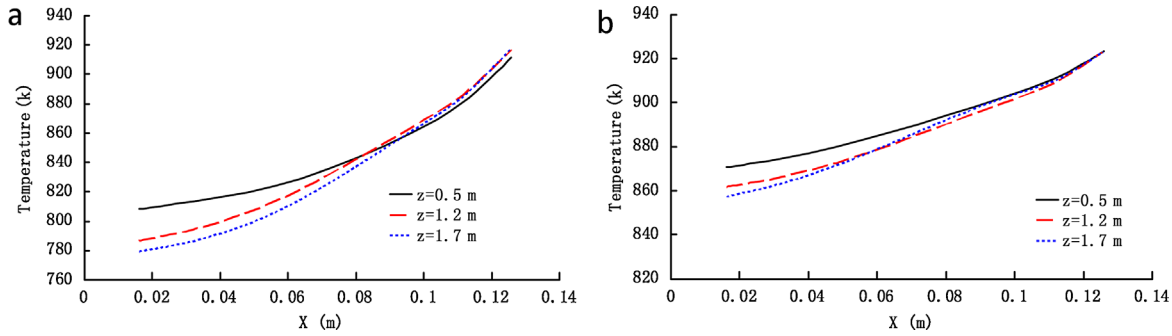

Figure 14. Distribution of gas temperature along the flow direction in catalyst bed at different heights of reactor with normal (a) and inverted cone (b) structures.

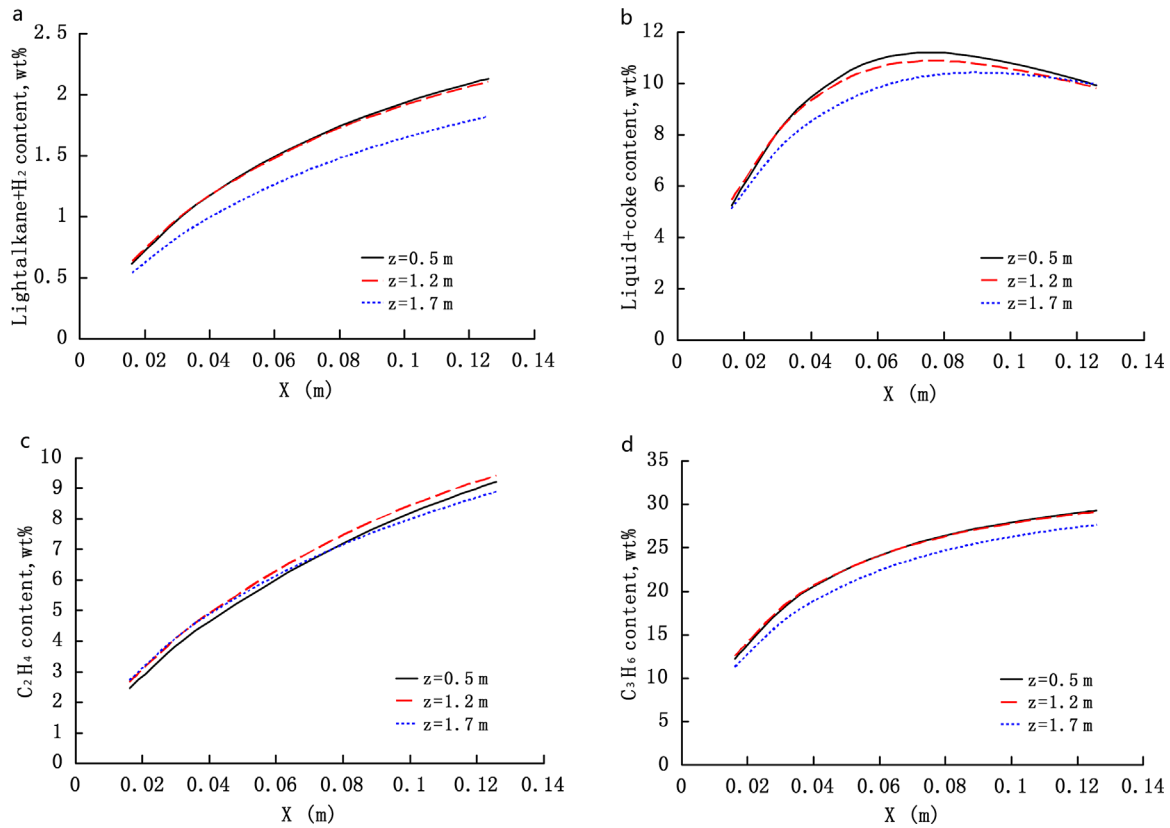

Figure 15. Distribution of species yield along the flow direction in catalyst bed at different heights of reactor with normal structure.

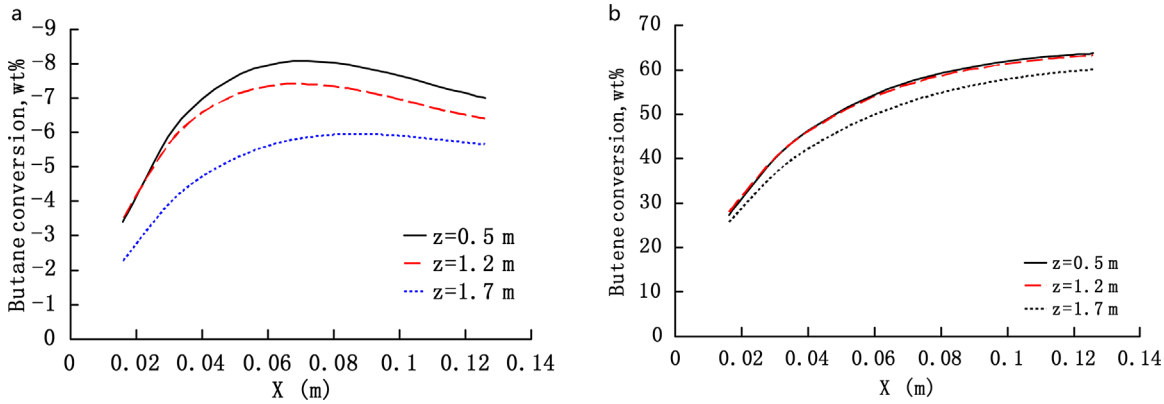

Figure 16. Distribution of reactant conversion along the flow direction in catalyst bed at different heights of reactor with normal structure.

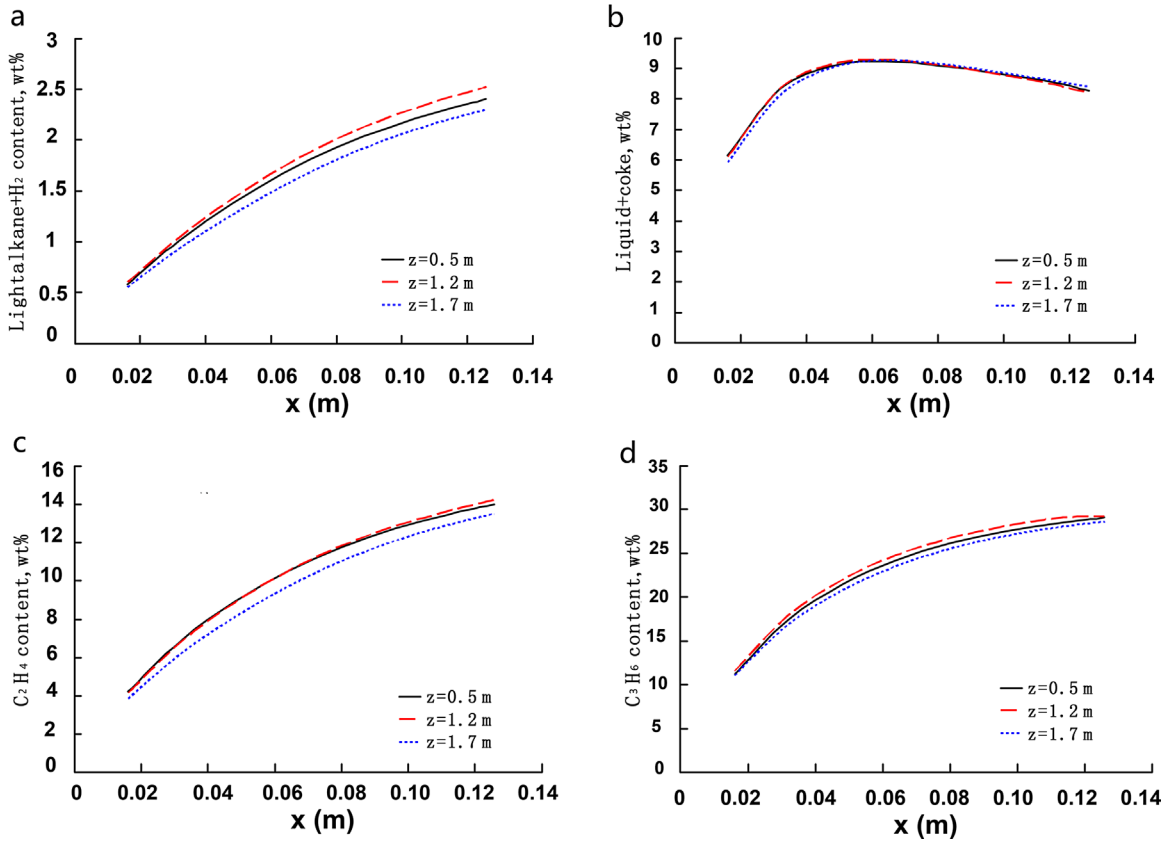

Figure 17. Distribution of species yield along the flow direction in catalyst bed at different heights of reactor with inverted cone structure.

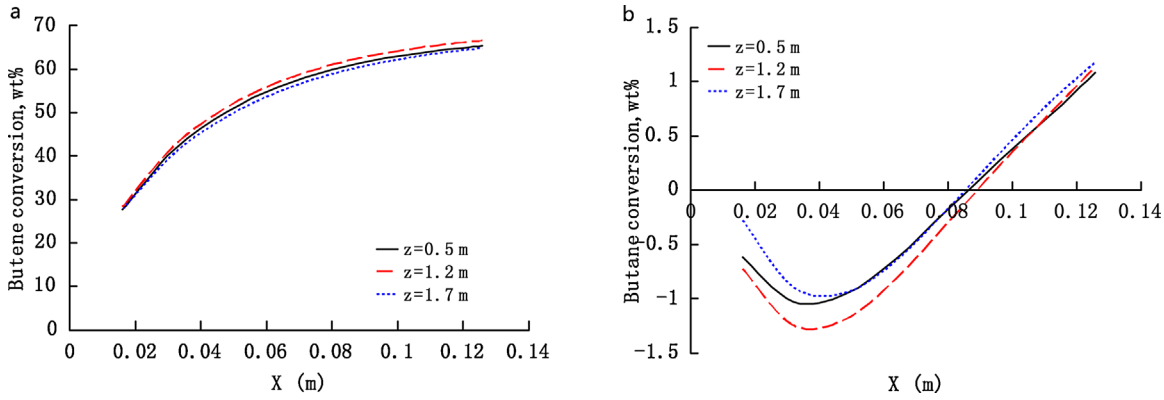

Figure 18. Distribution of reactant conversion along the flow direction in catalyst bed at different heights of reactor with inverted cone structure.

uniform than those with normal structure. In addition, using inverted cone structure enhances the ethylene and propylene yields due to a great increase of gas temperature in the first half of the catalyst bed. Furthermore, butane conversion changes from negative to positive because of the increase of gas temperature. Detailed information of axial difference of flow field and species conversion/yield is listed in Tables S12 and S13. From Tables S12 and S13, using an inverted cone structure can greatly shorten the axial difference of flow field and species conversion/yield, and increase the yields of ethylene and propylene.

As a whole, for the CP-Z radial moving bed reactor, the annular tube containing an inverted cone structure is sure to improve the uniformity of flow distribution, but the effect of inclination angle on the uniformity of flow distribution in the reactor remains to be investigated.

CONCLUSIONS

In this study, a comprehensive 3D CFD model coupled pyrolysis reactions was used to study the heat transfer performance of gas and solid phases and species concentration profiles in a CP-Z reactor. Effects of operation conditions and reactor structures on the flow field and the pyrolysis reactions were investigated. The following conclusions were drawn.

A good heat transfer performance between gas and solid phases in catalyst bed was identified. The temperature profiles are complex near the gas phase entrance side of the catalyst bed, especially in the middle part and at the bottom of the catalyst bed, and the temperature profiles have an obvious difference at different heights of reactor.

The product yields increase generally along the flow direction in catalyst bed, and there also exist some differences of species concentration profiles at different heights of the reactor.

Product yields are more sensitive to reaction temperature than to residence time. An initial catalyst temperature of 923.15 K and a width of catalyst bed in range of 0.119 m–0.139 m are preferable for a higher low-carbon olefins yields in this simulation.

For the CP-Z radial moving bed reactor, the annular tube containing an inverted cone structure positively improves the uniformity of flow distribution and low carbon olefins yields. However, the effect of inclination angle on the uniformity of flow distribution in reactor remains to be investigated.

ACKNOWLEDGEMENTS

The authors thank the National Ministry of Science and Technology of China (No. 2012CB21500402), the State Key Laboratory of Coal Conversion of China (No. J13-14-102), the Research Fund for the Doctoral Program of Higher Education (No. 20130073110077) and the State Key Laboratory of Chemical Engineering of Tsinghua University (No. SKL-ChE-13A05) for supporting this work.

NOMENCLATURE

α_g	volume fraction of gas phase
α_s	volume fraction of solid phase
α	permeability
ε	bed voidage
ρ_g	gas phase density (kg/m^3)
ρ_s	solid phase density (kg/m^3)
$\vec{V}_g$	gas phase velocity (m/s)
$\vec{V}_s$	solid phase velocity (m/s)
$\vec{u}_g$	gas phase weighted velocity (m/s)
P	pressure (Pa)
P_s	particle phase pressure (Pa)
$\bar{\bar{\tau}}_g$	shear stress of gas phase (N/m^2)
$\bar{\bar{\tau}}_s$	shear stress of solid phase (N/m^2)
$\bar{\bar{I}}$	identity matrix
K_{gs}, K_{sg}	interphase exchange coefficient of momentum (kg/m^3·s)
k_g	turbulence kinetic energy tensor of gas phase
k_{Θ_s}	diffusion coefficient for granular energy
g	gravitational acceleration (m/s^2)
g_0	radial distribution function
μ_g	gas viscosity (Pa·s)
μ_s	solid shear viscosity (Pa·s)
$\mu_{l,g}$	gas molecular viscosity (Pa·s)
$\mu_{t,g}$	turbulent viscosity of gas phase (Pa·s)
$\mu_{s,col}$	solid collision viscosity (Pa·s)
$\mu_{s,kin}$	solid kinetic viscosity (Pa·s)
$\mu_{s,fr}$	solid frictional viscosity (Pa·s)
λ_s	solid bulk viscosity (Pa·s)
λ	effective thermal coefficient (W/m·K)
Θ_s	granular temperature (m^2/s^2)
e_s	particle-particle restitution coefficient
d	particle diameter of porous media (m)
d_p	particle diameter of bed (m)
γ_{Θ_s}	energy collision dissipation of energy
φ_{gs}	energy exchange between gas and solid
θ	angle of internal friction (^{0})
I_{2D}	second invariant of the deviator stress tensor
C_D	drag coefficient
C_2	inertial resistant factor
$\vec{S}$	source term for the momentum equation
Re_s	particle Reynolds number
$\Pi_{k,g}$, $\Pi_{\varepsilon,g}$	influence of the dispersed phases on the continuous phase
C_μ, $C_{1\varepsilon}$, $C_{2\varepsilon}$	coefficients in turbulence model
G_{kg}	generation of turbulence kinetic energy due to mean velocity gradient in gas phase
ε_g	turbulence dissipation rate of gas phase
σ_g	turbulent Prandtl numbers for gas phase
σ_k	turbulent Prandtl numbers for k
σ_ε	turbulent Prandtl numbers for ε
D	mixed diffusion coefficient for CFD model (m^2/s)
Y_i	mass fraction of species i
Sc	Schmidt number
M_i	molecule weight of species i (kg/kmol)
h_g	enthalpy of gas phase (J/kg)
h_s	enthalpy of gas phase (J/kg)
T	temperature (K)
T_g	temperature of gas phase (K)
T_s	temperature of solid phase (K)
$k_{eff,g}$	thermal coefficient of gas phase (w/m·k)
$k_{eff,s}$	thermal coefficient of solid phase (w/m·k)
H_{sg}, H_{gs}	interphase exchange coefficient of energy (w/m3·k)
$\Delta H_{i,j}$	heat released by reaction i to j (kj/kmol)
R_i	rate of reaction i (kmol/m^3·s)
Nu_s	Nusselt number of solid phase
Pr	Prandtl number
$v_{i,j}$	ratio of molecule weight of species i and j
M_i, M_j	molecule weight of species i and j (kg/kmol)
Cp_i, Cp_j	heat capacity of species i and j (J/mol·k)
Cp	heat capacity of mixed gas phase (J/mol·k)

$\Delta_f H_i^\theta$, $\Delta_f H_j^\theta$	standard molar enthalpy of formation of species i and j (J/mol)
Mm	molecule weight of mixed species (kg/kmol)
(kg/kmol) k_i	reaction rate constant of lump i $(g/cm^3)^{-1}\cdot h^{-1}$
k_{0i}	pre-exponential factor
E_i	activation energy

REFERENCES

[1] C. Y. Li, C. H. Yang, H. H. Shan, *Ind. Eng. Chem. Res.* **2007**, *46*, 4916.

[2] X. X. Zhu, S. L. Liu, Y. Q. Song, L. Y. Xu, *App. Catal. A* **2005**, *288*, 134.

[3] K. K. Pant, D. Kunzru, *Ind. Eng. Chem. Res.* **1997**, *36*, 2059.

[4] M. Alyania, A. Mohamadalizadehb, J. Towfighia, N. Hosseinia, *J. Anal. Appl. Pyrolysis* **2012**, *98*, 7.

[5] A. Pinho, J. G. Furtado, P. P. Neto, J. A. Moreno, "Double riser FCC: An opportunity for the petrochemical industry," *NPRA Annual Meeting*, Salt Lake City, USA **2006**.

[6] S. H. Wang, *Ethylene Unit Technology*, Sino Petrochemical Publishing, Beijing **1994**.

[7] B. Basu, D. Kunzru, *Ind. Eng. Chem. Res.* **1992**, *31*, 146.

[8] L. Y. Wang, G. L. Wang, J. L. Wei, *Oil Gas J.* **2003**, *101*, 52.

[9] Y. G. Yang, Y. Luo, *Petrochem.* **2000**, *31*, 1.

[10] W. D. Han, R. K. Huang, J. H. Gong, *Pet. Refinery Eng.* **2006**, *36*, 1.

[11] L. Li, G. Wang, X. H. Meng, C. H. Xu, J. S. Gao, *Ind. Eng. Chem. Res.* **2008**, *47*, 710.

[12] S. M. Jeong, J. H. Chae, J. H. Kang, S. H. Lee, W. H. Lee, *Catal. Today* **2002**, *74*, 257.

[13] S. M. Jeong, J. H. Chae, W. H. Lee, *Ind. Eng. Chem. Res.* **2001**, *40*, 6081.

[14] X. B. Zhang, *Study on FCC gasoline deep catalytic cracking (in Chinese)*, Sino Petrochemical Publishing, Beijing **2007**.

[15] L. Li, J. S. Gao, C. M. Xu, X. H. Meng, *Chem. Eng. J.* **2006**, *116*, 155.

[16] C. Chen, B. Yang, J. Yuan, Z. W. Wang, L. Y. Wang, *Fuel* **2007**, *86*, 2325.

[17] X. H. Meng, C. M. Xu, L. Li, J. S. Gao, *Energy Fuel* **2010**, *24*, 6233.

[18] B. B. Jiang, X. Feng, L. X. Yan, Y. T. Jiang, Z. W. Liao, J. D. Wang, Y. R. Yang, *Ind. Eng. Chem. Res.* **2014**, *53*, 4623.

[19] Y. T. Jiang, C. J. Ren, Z. L. Huang, J. D. Wang, B. B. Jiang, J. Yang, Y. R. Yang, *Ind. Eng. Chem. Res.* **2014**, *53*, 4078.

[20] X. Q. Song, Z. W. Wang, Y. Jin, M. S. Gong, *Chem. Eng. Technol.* **1993**, *16*, 383.

[21] D. J. Gunn, *Int. J. Heat Mass Transfer* **1978**, *21*, 467.

[22] C. K. K. Lun, S. B. Savage, D. J. Jeffrey, N. Chepurniy, *J. Fluid Mech.* **1984**, *140*, 223.

[23] D. Gidaspow, *Multiphase flow and fluidization: Continuum and kinetic theory descriptions*, Academic Press, Boston **1994**.

[24] S. Ergun, *Chem. Eng. Prog.* **1952**, *48*, 89.

[25] J. S. Gao, C. M. Xu, S. X. Lin, G. H. Yang, *AIChE J.* **1999**, *45*, 1095.

[26] D. R. Stull, E. F. Westrum, G. C. Sinke, *The chemical thermodynamics of organic compounds,* John Wiley & Sons Inc., New York **1969**.

[27] L. Y. Carl, *Handbook of Thermodynamic Diagrams, Volume 1: C_1 to C_4 Compounds*, John Wiley & Sons Inc., New York **1996**.

[28] L. Y. Carl, *Handbook of Thermodynamic Diagrams, Volume 2: C_5 to C_7 Compounds*, John Wiley & Sons Inc., New York **1996**.

[29] D. G. Schaeffer, *J. Diff. Equ.* **1987**, *66*, 19.

[30] US 4980053 (**1990**) invs: Z. Li, S. Liu, X. Ge.

[31] F. R. Huang, M. Q. Wu, P. Du, Y. Jin, *J. Hydrodynamics (in Chinese)* **1999**, *6*, 107.

SUPPORTING INFORMATION

Additional Supporting Information may be found in the online version of this article at the publisher's web-site.

Manuscript received May 10, 2014; revised manuscript received July 14, 2014; accepted for publication July 26, 2014.